npg

ORIGINAL ARTICLE

New experimental rabbit animal model for cervical spondylotic myelopathy

G Klironomos[1], S Karadimas[1], A Mavrakis[1], P Mirilas[2], I Savvas[3], E Papadaki[4], DJ Papachristou[4,5] and G Gatzounis[1]

[1]Department of Neurosurgery, University of Patras, Patras, Greece; [2]Unit of Experimental Pediatric Surgery-Microsurgery, Second Department of Pediatric Surgery, Aristotle University of Thessaloniki, Papageorgio General Hospital, Thessaloniki, Greece; [3]Department of Anesthesiology, Animal Clinic, Faculty of Veterinary Medicine, Aristotle University of Thessaloniki, Thessaloniki, Greece; [4]Department of Anatomy-Histology-Embryology, University of Patras, Patras, Greece and [5]Department of Pathology, University of Pittsburgh, Pittsburgh, PA, USA

Study design: Cervical spondylotic myelopathy (CSM) represents the most commonly acquired cause of spinal cord dysfunction among individuals over 55 years old. The pathophysiology of the disease involves static and dynamic mechanical factors, which are the result of chronic degeneration. The clinical course of the disease remains unpredictable. In the past, many experimental animal models have been developed to study the cellular and molecular mechanisms underlining the pathophysiology of the disease.

Objectives: To create a new animal model of CSM, which will reproduce the temporal course of the disease and the local microenvironment at the site of spinal cord compression.

Methods: We performed posterior laminectomy to New Zealand rabbits at the level of C7, and a thin sheet (5–7 µm) of aromatic polyether was implanted with microsurgical technique at the epidural space underneath C5–C6 laminae. Motor function evaluation was performed after the operation and once a week thereafter.

Results: After 20 weeks, the animals were killed, and the histological evaluation of spinal cord at the site of compression above and below it, using eosin hematoxylin, immonohistochemistry and Kluver–Barrera techniques reveals axonal swelling and demyelination, interstitial edema and myelin sheet fragmentation. Moreover, histological evaluation of C5 and C6 laminae reveals osteophyte formation.

Conclusion: We believe that this CSM model reproduces the temporal evolution of the disease and creates a local microenvironment at the site of spinal cord compression, which shares the same characteristics with that of human disease.

Spinal Cord (2011) **49**, 1097–1102; doi:10.1038/sc.2011.71; published online 26 July 2011

Keywords: CSM; animal model; pathogenesis

Introduction

Cervical spondylotic myelopathy (CSM) is the most serious condition of cervical spondylosis, representing simultaneously the most commonly acquired cause of spinal cord dysfunction among individuals over 55 years old. Both static and dynamic factors are involved in this condition. Static factors represent acquired or developmental stenosis of the cervical vertebrate canal.[1] Dynamic factors are involved in repetitive damage on spinal cord, which aggravate the catastrophic effect of static factors and are the result of vertebral segmental instability.[2,3] These mechanical factors in turn converge in direct injury to neurons, axons and glial cells of the spinal cord via a

combination of events including ischemia, excitotoxicity, apoptosis and demyelination.[4,5] Histological studies on autopsy specimens have showed loss of neurons and vacuolar degeneration in the gray matter along with demyelination, myelin fragmentation and swelling of the axons in white matter.[6–8] Despite advances in diagnosis and surgical treatment of CSM, little is known about the cellular and molecular pathophysiology of the disease, and many patients still suffer from severe permanent neurologic deficits postsurgically. Therefore, it is not surprising that many studies have been conducted to establish an experimental model, which could efficiently reproduce myelopathy reflecting the disease process seen in humans and thus, to be useful in the investigations of myelopathy due to chronic spinal cord compression.[9]

Herein, we present a new experimental rabbit model for CSM, using a synthetic aromatic polyether as the gradually

compression material of cervical spinal cord. In our effort to assess if this new model reproduces the pathological features of CSM, we evaluated histological, histochemical and immunohistochemical parameters in the spinal cord of 15 rabbits with CSM and in 15 control animals, and assessed possible differences between the two groups.

Materials and methods

Experimental animals
Thirty 8-week-old New Zealand rabbits weighing 2.5–3.5 kg were used in this study. The animals were kept in cages at 18–22 C°, with a 12 h light/12 h dark cycle, and were allowed to move freely inside the room twice a day. They were given an ordinary laboratory diet and water. Before surgery, the animals were kept in their cages to get familiar with the environment. Throughout the entire study, the animals were kept in their cages under pathogen-free conditions, with regulated air and humidity conditioning under the supervision of a veterinarian. Our study protocol has been reviewed and approved by the Bioethical Committee Aristotle University of Thessaloniki.

Experimental groups
For the present study, we used 30 rabbits that were divided to the following two groups. The first group ($n=15$) was the control group, which involved animals that underwent sham surgery with the passage, but not implantation of the compressive material. The second group ($n=15$), the 'compression group' involved animals that underwent aromatic polyether sheet implantation (see below). All animals were perfused 20 weeks after surgery.

Surgical procedure
A total of 15 animals underwent posterior lower cervical laminectomy, with microsurgical technique under surgical microscope and sterile conditions. The procedure was performed under general intravenous anaesthesia using propofol ($2.5 \, mg \, kg^{-1}$). A laryngeal mask was used for mechanical ventilation. An antibiotic agent (Cefazolin) was administrated intravenously at the beginning of the operation. The animals were positioned on the operating table lying on face down and immobilized. Fur on cervical area was shaved; the area was scrubbed and sterilized with sterilium and a midline longitudinal incision was performed. Under X-ray, we identified the lower cervical spinous process performed and the paravertebral muscles were stripped from the spinous process. C7 lamina and the yellow ligaments C6–C7 and C7–C8 were removed. With a microhook, periosteal removal of the inner surface of C6 lamina was performed. A small sheet of aromatic polyether (0.5 cm width, 1 cm length, 0.7 mm thick) sterilized at 120°C was introduced under C6 laminae at the epidural space. The wound was closed in anatomic order, using dexon suture for cervical aponeurosis and nylon for dermal closure. At the end of the procedure, an analgetic agent (Paracetamol) was given intramuscularly. The animals allocated to the control group ($n=15$) were subjected to laminectomy and the

aromatic polyether was placed underneath the laminae once and then removed (sham operation). Before and during the procedure, electrophysiological monitoring was performed and no changes in wave pattern were detected. The day after the operation, the walking pattern of the examined animals was normal.

Compression material
As compressive material, we used a 0.5–0.7-mm thick, fine sheet of aromatic polyether.[10] The most characteristic property of this material is its capacity to absorb phosphate anions and induce new bone formation. Moreover, aromatic polyether has the ability to increase calcium phosphate sedimentation. Previous studies have showed that this material accelerates bone fracture healing.[10]

Motor function evaluation
Motor function was evaluated by using the modification of Tarlov's classification (Table 1). Evaluation was made before and immediately after the surgery, and once a week thereafter.

Tissue preparation and immunochemistry
All the animals were perfused 20 weeks after the operation. Spinal cord and cervical vertebral column from each animal was extirpated immediately after perfuse. Surgically removed spinal cord tissue was fixed in 10% buffered formalin and embedded in paraffin. Section of 4 μm thick were obtained from each paraffin block and placed on SuperFrost (Menzel-Gläser, Braunschweig, Germany) plus glass slides. After deparaffinization and rehydration in graded alcohols, hematoxylin–eosin and Kluver–Barrera histological stainings were applied. Moreover, conventional immunohistochemistry was performed using the two-step peroxidise technique, with a peroxidase-conjugated polymer (DAKO Envision kit, DAKO, Carpinteria, CA, USA). The primary antibodies that were used are described in details in Table 2. Sections were counterstained with Harris' hematoxylin, dehydrated and

Table 1 Tarlov's classification

Grade	Motor characteristics
0	Unable to have voluntary movements
1	Perceptible movements at joints, the hindlimbs follow
2	Good movements to joints, but unable to stand up
3	Can stand up and walk, but unable to start running quickly
4	Normal

Table 2 Immunohistochemistry protocol characteristics

Antibody	Source	Antigen retrieval	Dilution	Incubation
NF	Cell Marque	Microwave	1:40 in TBS–BSA	Overnight
S100	Cell Marque	Microwave	1:30 in TBS–BSA	Overnight
GFAP	Neo Marker	Microwave	1:40 in TBS–BSA	Overnight

Abbreviations: BSA, bovine serum albumin; GFAP, glial fibrillary acidic protein; NF, neurofilaments; TBS, tris-buffered saline.

mounted permanently. Finally, vertebral arch slices underwent hematoxylin–eosin staining.

Immunohistologic evaluation

Each slide was independently evaluated by one experienced pathologist (EP) and one investigator (GK). The evaluators were blinded to the study groups. The intensity of the immunostaining for all the antibodies was scored as follows: $3+$, normal staining; $2+$, moderate staining; $1+$, weak staining and 0, negative staining. The distribution of immunostaining was scored according to the following assumption: $3+$, >80% of cells display positive immunoreactivity; $2+$, 30–80% of cells display positive immunoreactivity; $1+$, 10–30% of cells display positive immunoreactivity; and 0, <10% of cells display positive immunoreactivity for the examined protein. The total score combined the intensity and the distribution of immunostaining was calculated as follows: 1: intensity 0, $1+$ and distribution of staining 0, $1+$, $2+$, $3+$ or intensity $2+$ and distribution $1+$; 2: intensity $2+$ and distribution $2+$, $3+$ or intensity $3+$, distribution $2+$, $3+$.

Kluver–Barrera staining was used to evaluate the extent of myelin damage in sites of myelopathy, in comparison with normal spinal spinal cord.

Statistical analysis

Statistical analysis was performed using 12.0 SPSS for Windows (SPSS Inc., Chicago, IL, USA). To test the significance of differences of the protein expression levels between the two experimental groups, we performed Mann–Whitney tests. The significance level was defined as $P < 0.05$.

Results

Evaluation of animals

Clinical evaluation of animals after operation reveals no symptoms and signs of acute spinal cord injury. The motor function level of animals, which underwent the implantation of the compression material, was gradually decreased throughout the 20 weeks. The motor function level just before the killing was graded as '3' in 7 out of 15 myelopathic animals, and graded as '2' in 8 out of 15 myelopathic animals. In contrast to the above data, the motor function level was grade 4 in all of the control animals throughout the whole period of the experiment.

Evaluation of spinal cord specimens

Gross appearance of spinal cord reveals flattening at the anterior–posterior direction at the site of material implantation, indicating chronic compression (Figures 1a–c). Histological evaluation demonstrated characteristic lesions of chronic myelopathy. More specifically, hematoxylin–eosin staining revealed that at the compression site, spongy degeneration in white matter was observed. In the gray matter, we observed flattening of the anterior horn, neuronal ischemic changes and alterations of anterior horn cells, such as nuclear centralization, dense nucleoli and Nissl chromatolysis (Figures 2a and b).
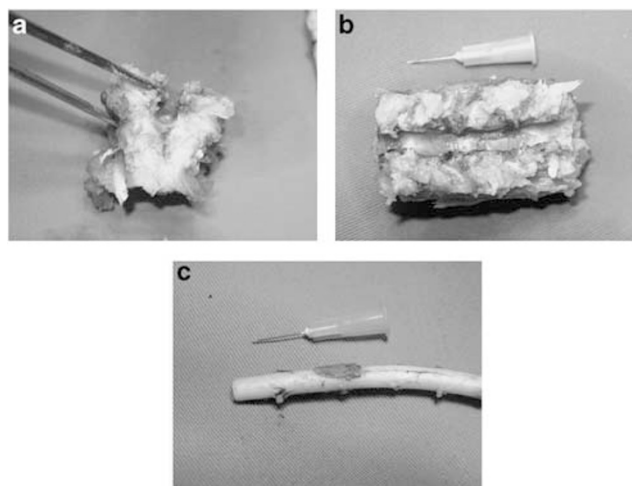

Figure 1 (**a**) Tranverse section of vertebral body demonstrates osteophyte formation, (**b**) Saggital section of vertebral body. Vertebral canal stenosis was produced by osteophyte. (**c**) Spinal cord compression at the site of material insertion.
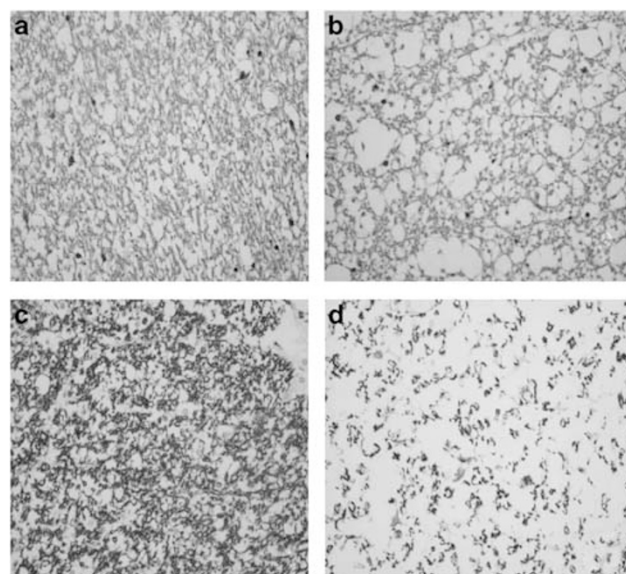

Figure 2 (**a**) Hematoxylin–eosin (HE) staining of normal spinal cord. (**b**) HE staining of spinal cord at the site of compression reveals interstitial edema and vacuolar degeneration. (**c**) Kluver–Barrera (KB) staining of normal spinal cord. (**d**) KB staining of spinal cord at the site of compression reveals spinal cord edema, myelin sheath fragmentation, axon swelling (enlargement of myelin rings) and demyelination.

Kluver–Barrera staining evaluation

Kluver–Barera staining reveals myelin sheath fragmentation, enlargement of myelin ring and decrease width of myelin findings that strongly suggest demyelination (Figures 2c and d).

NF protein expression

In spinal cord specimens obtained from control animals, enhanced immunostaining for neurofilaments (NF) was

observed in 14/15(93.3%) the cases. On the contrary, low cytoplasmic expression of NF was observed in all the spinal cord specimens derived from animals with CSM, but only in 1/15 (6.6%) of the non-myelopathic animals. Mann–Whitney test revealed that the expression levels of NF were significantly lower ($P = 0.001$) in animal with CSM, compared with the controls (Figures 3a and b).

S-100 protein expression

Strong cytoplasmic expression of S100 was observed in the spinal cord specimens of all the control animals 15/15 (100%); nonetheless, high S100 protein expression was detected in only 2/15 (13.3%) spinal cord specimens from myelopathic animals. Weak S100 immunostaining was detected in 13/15 (86.6%) of myelopathic animals, but in none (0%) of the control animals. The expression levels of S100 were significantly higher in the control animals ($P = 0.001$), as compared with CSM rabbits (Figures 3c and d).
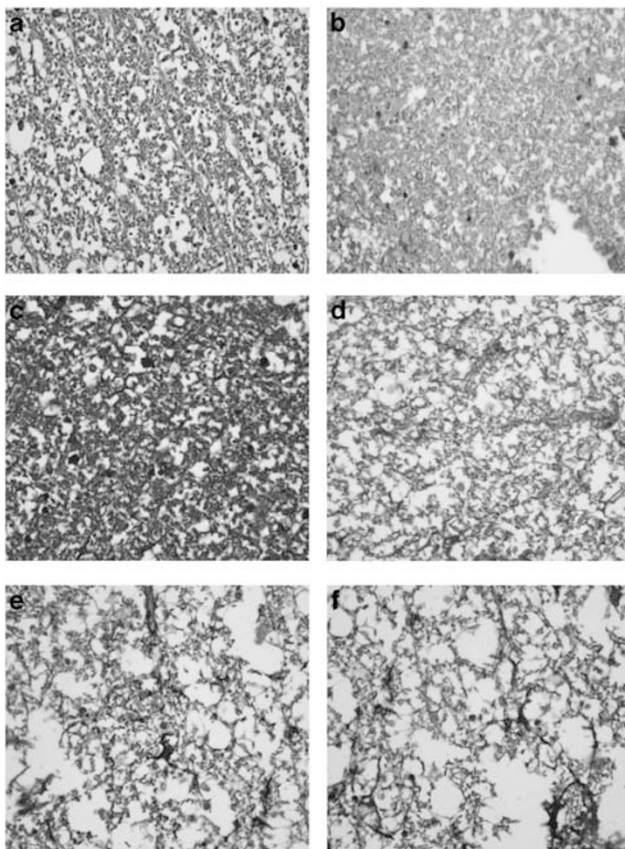

Figure 3 (**a**) Immunohistochemical staining of normal spinal cord with anti-NF antibody. (**b**) Immunohistochemical staining of compressed spinal cord with anti-NF antibody demonstrates interstitial edema, axonal swelling and decreased intensity of the staining. (**c**) Immunohistochemical staining of normal spinal cord with anti-S-100 antibody. (**d**) Immunohistochemical staining of compressed spinal cord with anti-S-100 antibody reveals significant demyelination. (**e**) Immunohistochemical staining of normal spinal cord with anti-GFAP antibody (**f**) Immunohistochemical staining of compressed spinal cord with anti-GFAP antibody shows interstitial edema.

GFAP protein expression

Immunohistochemical analysis revealed weak cytoplasmic immunoreactivity for glial fibrillary acidic protein (GFAP) in 15/15 (100%) of the control, but in 3/15 (20%) of the diseased animals. High cytoplasmic expression was not detected in any of the control animals. However, it was observed in 12/15 (80%) of myelopathic animals. Statistical analysis revealed that the expression levels of GFAP were significantly higher in CSM, compared with the control group (Figures 3e to f).

Histologic evaluation of vertebral arch at the site of material insertion

Histological evaluation of vertebral arch at the site of material implantation was performed using hematoxylin–eosin staining. No evidence of tissue reactions such as inflammation or granulation tissue surrounding the implant was observed. Interestingly, at the site of material implantation, we observed numerous activated osteoblasts, chondroblasts, as well as newly formed osteoid (Figure 4).

Discussion

CSM is a very common manifestation of cervical spondylosis. Despite the severity of the disease, very few studies have been conducted in order to investigate the pathobiology of this disease.[8,11–13] In the present study, we present a new animal model of CSM that simulates the temporal profile, as well as the local microenviroment of the disease. In order to assess the presence and the extent of the demyelination in the present model, we performed the myelin-specific Kluver–Barrera histochemical staining. Our findings showed that the demyelination of axons was dramatically increased in CSM, compared with normal tissues.

In order to document the presence of myelopathic changes of the examined animals, we performed a series of immunohistochemical analyses and had several notable results. More specifically, the expression levels of S-100 in the spinal cord specimens derived from animals with CSM were significantly weaker in comparison with the cellular levels of S100 in the control animals. Our data are in symphony with previous autopsy studies of the cervical spinal cord subjected to long-term compression, having shown myelin destruction, loss of axons and oligodendrocytes, and sub-
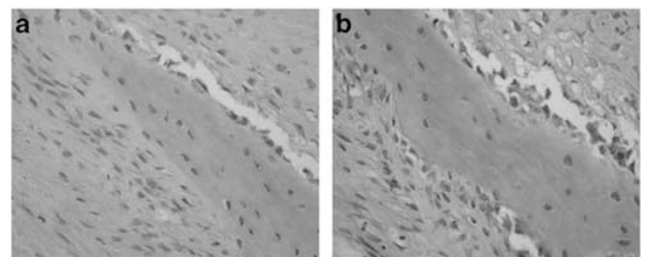

Figure 4 (**a**, **b**) Hematoxylin–eosin staining of osteophyte demonstrates osteoblasts proliferation, and new osteoid formation.

sequent demyelination of the ascending and descending tracts.[14]

In the present study, we showed that the cellular levels of NF were significantly lower in the myelopathic, as compared with normal spinal cords. It is known that the morphologic stability and plasticity of neuronal processes depend upon the integrity of the neuronal cytoskeleton and its components (that is, actin filaments, neurofilaments, microtubules and their associated proteins).[15] Neurofilaments are key structural elements of the white matter axons and represent a very important group of structural proteins, which support the architecture of the axons of peripheral and central nervous system.[16] Our results suggest that the proposed animal model reproduces the insidious loss of neurofilaments indicating axonal degeneration, which is one of the main histopathological features of human CSM.

Our experiments also showed that GFAP expression levels were significantly higher in the pathological tissues compared with the normal tissues. Glial scar is usually observed after CNS lesions and consists mainly of reactive astrocytes. Histopathologically, it is characterized by intense GFAP immunostaining. In addition to forming a non-permissive physical barrier to the regenerative axons, glial scar also secretes inhibitory molecules such as chondroitin sulfate proteoglycans, which chemically arrest the re-growth of injured axons across the lesion.[17] Formation of the glial scar is a complex process that is primarily attributed to astrocyte aggregation in the vicinity of the lesion. Astrocyte proliferation also contributes to this process.[18–21] The expression pattern of GFAP in the tissues evaluated in our study indicates that there is an extensive aggregation of reactive astrocytes in the pathological tissues in contrast to normal tissues. The astrocytes aggregation and proliferation is the premature phase of the glial scar formation, which is one of the main histopathological features of human CSM.

Various animal experiments have been conducted in order to deepen the understanding on the pathology and pathophysiology of the CSM. In Kim et al.[20] model, the compressive material has a rapid expansion rate during the first 24 h and after that, it remains stable compressing constantly the spinal cord. Additionally, the local microenvironment at the compression site does not resemble human CSM. In the experimental model proposed by Kanchiku et al.[21] there is a more realistic temporal profile of compressing force on spinal cord, but the manner by which the compression takes place does not correspond to human disease. Therefore, in the aforementioned models, the characteristic temporal profile of the disease as well as the local microenvironment at the site of spinal cord compression may not be adequately reproduced. In contrast to the previous models, our model has specific advantages. First, it reproduces the clinical course and the characteristics of human CSM that include absence of acute myelopathy or immediate neurological deficit after induction of cord compression, insidious and delayed onset of symptoms and progression once the process becomes symptomatic due to the distinctive characteristics of the used material. Second, it recapitulates the histopathological characteristics of human CSM, which are demyelination, axonal degeneration and

glial scar formation. Third, in this study, we demonstrate for the first time osteoid formation, fibroblasts, chondrocytes and osteoblasts presence at site of material insertion, findings that suggest active bone remodeling. This finding suggests that in our model, the mechanism of spinal cord compression is based upon the formation of new osteophyte, resembling the local microenvironment of the compression site of human CSM.

In summary, our findings suggest that the proposed model ensures a local microenvironment at the site of spinal cord compression that resembles human CSM and mimics spatial and temporal profile of the disease. Clearly, additional studies at the cellular and molecular levels are needed to understand the mechanisms that are responsible for the pathogenesis of this devastating disease.

Conflict of interest

The authors declare no conflict of interest.

Acknowledgements

References

1 Imai T. Cervical spondylotic myelopathy and sagittal diameter of the cervical canal]. Nippon Seikeigeka Gakkai Zasshi 1970; 44: 429–438.

2 White III AA, Panjabi MM. Biomechanical considerations in the surgical management of cervical spondylotic myelopathy. Spine 1988; 13: 856–860.

3 Robinson RA, Afeiche N, Dunn EJ, Northrup BE. Cervical spondylotic myelopathy: etiology and treatment concepts. Spine 1977; 2: 89–99.

4 Baptiste DC, Fehlings MG. Pathophysiology of cervical myelopathy. Spine J 2006; 6: 190S–197S.

5 Barron EM, Young WF. Cervical spondylotic myelopathy: a brief review of its pathophysiology clinical course, and diagnosis. Neurosurgery 2007; 60(1 Supp1 1): S35–S41.

6 Barnes MP, Saunders M. The effect of cervical mobility on the natural history of cervical spondylotic myelopathy. J Neurol Neurosurg Psychiatry 1984; 47: 17–20.

7 Hogan El, Romanul FCA. Spinal cord infarction occurring during insertion of aortic graft. Neurology 1966; 16: 67–74.

8 Mair WGP, Druckman R. The pathology of spinal cord lesions and their relation to the clinical features in protrusion of cervical intervertebral discs (a report of four cases). Brain 1953; 76: 70–91.

9 Karadimas SK, Gialeli CH, Klironomos G, Panagiotopoulos E, Karamanos NK et al. The role of oligodendrocytes in the molecular pathobiology and potential molecular treatment of cervical spondylotic myelopathy. Curr Med Chem 2010; 17: 1048–1058.

10 Tyllianakis M, Dalas E, Christofidou M, Kallitsis JK, Chrissanthopoulos A, Koutsoukos PG et al. Novel composites materials from functionalized polymers and silver coated titanium oxide capable for calcium phosphate induction, control of orthopedic biofilm infections: an 'in vitro' study. J Mater Sci Mater Med 2010; 21: 2201–2211.

11 Ito T, Oyanagi K, Takahashi H, Takahashi HE, Ikuta F. Cervical spondylosis myelopathy: clinicopathologic study on the progression pattern and thin myelinated fibers of the lesions of seven patients examined during complete autopsy. Spine 1996; 21: 827–833.

12 Ogino H, Tada K, Okada K, Yonenobu K, Yamamoto T, Ono K *et al*. Canal diameter, antero-posterior compression ratio, and spondylotic myelopathy of the cervical spine. *Spine* 1983; **8**: 1–15.

13 Payne LW, Spillane JD. The cervical spine, an anatomical study of 70 specimens, with particular reference to the problem of cervical spondylosis. *Brain* 1957; **80**: 571–596.

14 Fehlings MG, Yu WR, Shannon P, Sekhon LHS. Molecular mechanisms of cell death in human cervical spondylotic myelopathy: evidence for apoptosis, death receptor expression and Caspase 3 activation. *Proceedings of the 28th Annual Meeting of the Cervical Spine Research Society* 2000.

15 Silver J, Miller JH. Regeneration beyond the glial scar. *Nat Rev Neurosci* 2004; **5**: 146–156.

16 Ridet JL, Malhotra SK, Privat A, Gage FH. Reactive astrocytes: cellular and molecular cues to biological function. *Trends Neurosci* 1997; **20**: 570–577.

17 Fitch MT, Doller C, Combs CK, Landreth GE, Silver J. Cellular and molecular mechanisms of glial scarring and progressive cavitation: *in vivo* and *in vitro* analysis of inflammation-induced secondary injury after CNS trauma. *J Neurosci* 1999; **19**: 8182–8198.

18 McGraw J, Hiebert GW, Steeves JD. Modulating astrogliosis after neurotrauma. *J Neurosci Res* 2001; **63**: 109–115.

19 Matyash M, Matyash V, Nolte C, Sorrentino V, Kettenmann H. Requirement of functional ryanodine receptor type 3 for astrocyte migration. *FASEB J* 2002; **16**: 84–86.

20 Kim P, Haisa T, Kawamoto T, Kirino T, Wakai S. Delayed myelopathy induced by chronic compression in the rat spinal cord. *Ann Neurol* 2004; **55**: 503–511.

21 Kanchiku T, Taguchi T, Kaneko K, Yonemura H, Kawai S, Gondo T. A new rabbit model for the study on cervical compressive myelopathy. *J Orthop Res* 2001; **19**: 605–613.